On the Feasibility of Using IEEE 802.11ad mmWave for Accurate Object Detection*

Hossein Ajorloo, Cormac J. Sreenan
Department of Computer Science
Cork, Ireland
hossein.ajorloo@ucc.ie
cjs@cs.ucc.ie

Adrian Loch, Joerg Widmer
IMDEA Networks Institute
Madrid, Spain
firstname.lastname@imdea.org

ABSTRACT

Millimeter wave (mmWave) bands are considered highly for localization and object detection. In this paper we assess the potential of commercial IEEE 802.11ad mmWave equipment to offer accurate object detection, ultimately providing models of the physical environment. Unlike solutions using bespoke mmWave equipment for detection, the use of IEEE 802.11ad ensures a low-cost system, and one in which detection can be integrated with communication, creating potential for innovative applications. Our approach is to build a laboratory testbed in which we capture reflected mmWave signals that are generated and transmitted by a commercial off-the-shelf (COTS) IEEE 802.11ad mmWave device. From the measured channel impulse response, we measured the distance from the mmWave transceiver to the objects in the environment, by some simple signal processing techniques. By knowing the angle of mmWave departure/arrival and this measured distance, we can develop a 2D model of the physical environment. We report on the achieved accuracy, which is 2cm in most experiments, and discuss technology limitations and research opportunities.

1 INTRODUCTION

mmWave technology is perceived as one of the key enablers of 5G [16]. Directional array antennas are used in mmWave wireless communications to compensate for free space path loss [2]. Beamforming and beamsteering are used to electronically steer antenna beams [3]. mmWave technology enables large bandwidth demanding applications such as autonomous vehicles [9] and augmented/virtual reality [1]. mmWave radar detection potential can be merged with the communication potential to enhance the performance of these applications.

For this purpose, in this paper we propose to use 802.11ad frames for detection which facilitates joint communications/detection and allows COTS hardware. This is cheaper than a bespoke detection solution using mmWave sensors, e.g. [8]. We use the preamble of IEEE 802.11ad and channel estimation to detect reflections from large objects in the environment and measure their distance to the mmWave transceiver. This can be used to detect the communicating devices and objects within the environment which is modeled by a 2D/3D map in real time and use this information to enhance the communication performance. In some applications such as vehicular communication, the detection potential is also used for detecting objects to avoid collision. There are numerous ideas to use this joint ranging-communication, e.g. for enhancing the antenna training and tracking protocols and predicting blockage of the communication channel by moving objects and human. Other technologies such as laser or infrared are also used for object detection. However, they are not integrated in 5G and smart phones, while mmWave has already been adopted for communications in 5G. Using mmWave detectors requires other circuitry to be included in the smart phones or other wireless network devices which makes them more expensive. To the best of our knowledge, these are the first experiments that use the channel impulse response (CIR) of a COTS IEEE 802.11ad transmitter for accurate object detection, which is the main contribution of this paper.

The rest of this paper is organized as follows: section 2 gives a brief overview of the related work. In section 3 we summarize the background and methodology. We then present the details of our experimental setup and results in section 4. Our observations and the main recognized challenges are summarized in section 5. Finally, section 6 concludes this paper and provides some notes on our plan for future work.

2 RELATED WORK

Some authors report localization/detection techniques in mmWave band which are evaluated in a simulation environment and almost all of them assume an ideal disc flat antenna pattern model. Cui et al. [5] examined vehicle positioning using 5G mmWave signals. Both a correlation receiver and an energy detector were considered for timing estimation. Olivier et al. [15] designed algorithms based on angle difference-of-arrival and location fingerprinting. Lemic et al. [11] examined a set of feasible localization approaches in the context of mmWave bands and found requirements for future mmWave devices. Talvitie et al. [20] proposed a method for estimation of the user equipment (UE) position and antenna orientation. Based on these estimated channel parameters, they formulate an iterative Gibbs sampler to obtain statistical descriptions for the unknown UE position and orientation. Shahmansoori et al. [17] proposed an algorithm for position and rotation angle estimation using signals from a single transmitter. Lin et al. [12] proposed to use a joint received signal strength (RSS) and angle of arrival positioning scheme for positioning in mmWave. Recently, Kumari et al. [10] used simulation techniques to motivate the use of IEEE 802.11ad preambles for the purpose of radar detection. Bocquet et al. [4] proposed a mmWave positioning system operating in indoor environments and using broadband impulse signals. Yang et al. [23] measured vital signs such as heart beat and breathing rates using an experimental setup based on a signal generator and signal analyzer. They used received signal strength of the mmWave signal reflected

*This project has received funding from the European Union's Horizon 2020 research and innovation programme under the Marie Sklodowska-Curie grant agreement No 713567. This publication has emanated from research supported in part by a research grant from Science Foundation Ireland (SFI) under Grant Number 13/RC/2077.

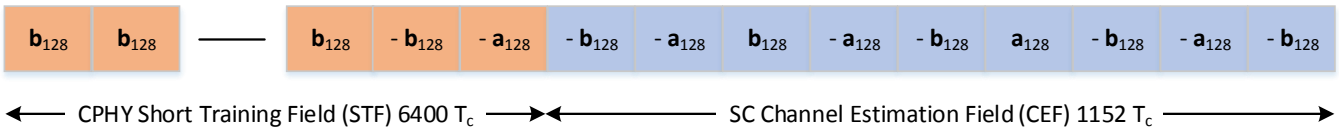

Figure 1: Preamble of IEEE 802.11ad control frames expressed in terms of Ga_{128} and Gb_{128} sequences [22].

off a human body and find peaks in the frequency domain of the reflected signal strength.

There are some reports on using software defined radio (SDR) for localization in the wireless networks. Dobbins et al. [6] implemented a localization system using USRP SDR and GNU Radio. Both time of arrival and received signal strength methods are used by an array of wireless receivers to trilaterate a cooperative transmitter. Nambiar et al. [14] used least squares localization techniques for finding the target device's location. Guo et al. [7] used multiple fingerprints, namely RSS, covariance matrix, signal subspace, fractional low-order moment, and fourth-order cumulant, which are obtained by different transformations of the received signals from multiple antennas and used neural network classifiers to localize the transmitter based on the learned fingerprints. However, all of these works are done in lower frequency bands between 900MHz-5.7GHz. But we aim at using active detection techniques instead of passive signal analysis techniques used by these methods.

3 BACKGROUND AND METHODOLOGY

In this section, we briefly explain the background of our method to measure the distances between the transceiver and the objects in the environment from which the mmWave reflects. We include our methodology of how we use channel estimation for this purpose. Channel estimation is a method used to estimate the wireless communication channel properties in particular, the multipath effects, at each time. In theory, this is equivalent to send an impulse signal through the channel and measure the channel effects on it, i.e., the channel impulse response.

For the channel estimation, IEEE 802.11ad uses Golay complementary sequences in the preamble of the frames. Golay complementary sequences are pairs of sequences of bipolar symbols (±1) that have been mathematically constructed to have very specific autocorrelation properties. They are used extensively in 802.11ad for a variety of purposes. In a receiver, correlators are used to detect a specific transmitted sequence [21]. This sequence is known by both sides of transmitter and receiver and is included in the preamble of each 802.11ad frame which is used for channel estimation. Channel estimation is based on sequentially passing the two sequences in a Golay complementary pair through the channel and combining the results. We have two time sequences, a and b. If we pass sequence a through the channel H, we convolve the sequence and the CIR, $h(t)$. If we pass the received signal through a Golay correlator for the known input sequence, then we get the autocorrelation of sequence a convolved with the CIR. If sequence b is processed similarly, we get the autocorrelation of sequence b convolved with the same CIR. If we add the two results together then, because sequences a and b are Golay complementary sequences, the sum of their autocorrelations is an impulse response and we are left with the CIR, $h(t)$ [21].

The control frame types such as beacon frames have a preamble structure comprising a Short Training Field (STF) followed by a Channel Estimation Field (CEF). These fields are constructed from $\pi/2$-BPSK modulated repeating Golay sequences. Figure 1 shows the structure of the control frame preamble in more detail, illustrating that the basic building blocks are the Golay complementary sequences $\mathbf{a}_{128}$ and $\mathbf{b}_{128}$ [22]. A pair of Golay sequences $\mathbf{a}_N$ and $\mathbf{b}_N$ and of length N, where N is a power of 2, has the following autocorrelation property [13]:

$$\mathbf{R}_a[i] + \mathbf{R}_b[i] = 2N\delta[i], \tag{1}$$

where

$$\mathbf{R}_a[i] = \sum_{n=0}^{N-i-1} \mathbf{a}_N[n+i] \times \mathbf{a}_N^*[n],$$
$$\mathbf{R}_b[i] = \sum_{n=0}^{N-i-1} \mathbf{b}_N[n+i] \times \mathbf{b}_N^*[n]. \tag{2}$$

A complete digital time-domain Golay-sequence aided channel estimation is proposed by Liu et al. [13]. Here, we briefly explain their approach. They compute CIR as

$$\mathbf{h}_{\text{est}}[i] = \frac{1}{4}\Big(\hat{\boldsymbol{\alpha}}[i] + \hat{\boldsymbol{\alpha}}[i+512] + \hat{\boldsymbol{\beta}}[i] + \hat{\boldsymbol{\beta}}[i+512]\Big), \tag{3}$$

where

$$\hat{\boldsymbol{\alpha}}[i] = \boldsymbol{\alpha}[i+N_{CP}], \qquad i = 0, \ldots, 767,$$
$$\hat{\boldsymbol{\beta}}[i] = \boldsymbol{\beta}[i+N_{CP}+256], \qquad i = 0, \ldots, 767, \tag{4}$$

in which N_{CP} denotes channel estimation sequence (CES) cyclic prefix and postfix length. In Eq. (4),

$$\boldsymbol{\alpha}[i] = \frac{1}{256}\sum_{n=0}^{255} \mathbf{r}_{\text{CES}}[i+n] \times \mathbf{a}_{256}^*[n],$$
$$\boldsymbol{\beta}[i] = \frac{1}{256}\sum_{n=0}^{255} \mathbf{r}_{\text{CES}}[i+n] \times \mathbf{b}_{256}^*[n], \tag{5}$$

where $\boldsymbol{\alpha}[i]$ and $\boldsymbol{\beta}[i]$ are the correlation values between the received CES and Golay sequences $\mathbf{a}_{256}$ and $\mathbf{b}_{256}$. In Eq. (5), $\mathbf{r}_{\text{CES}}[i]$ is the received i^{th} sample $\mathbf{r}_{\text{CES}}$ in CES field.

The channel estimation output is a complex number sequence. When we plot the magnitude of the estimated CIR in the time domain, we see some peaks which correspond to different paths from transmitter to receiver. So we can determine the spread of path delays between two different paths. This means that in a setup where the transmitter and receiver are located close to each other and the transmitter transmits toward an object and the receiver

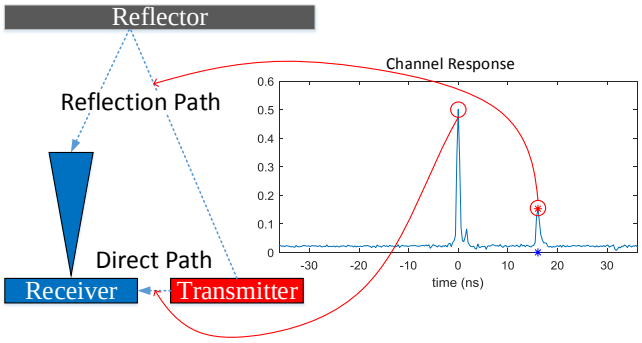

Figure 2: The setup for object distance measurement based on IEEE 802.11ad CIR.

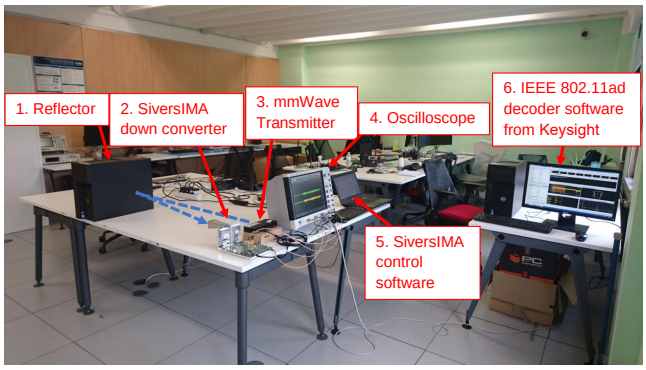

Figure 3: Basic experimental setup to check the feasibility of mmWave distance measurement based on reflection of IEEE 802.11ad beacon frame from a metal reflector in a laboratory environment.

receives this reflected signal, it can see at least two peaks in its channel estimation sequence: one corresponding to the direct path from transmitter to receiver and one from the reflection from the object (see Figure 2). The peak of the direct path is visible even if directional beam-patterns are being used to transmit and receive due to the sidelobes of the beam-patterns. By measuring the time difference between these two peaks, and considering the speed of light, we can measure the distance between the transmitter-receiver pair and the object. For the radar detection purpose by this method, the transmitter and receiver should be the same, which means that the device should be able to work in full-duplex mode.

4 EXPERIMENTAL SETUP AND RESULTS

Our basic experimental setup is shown in Figure 3. We use a Keysight DSOS254A (number 4 in Figure 3) which is a high-definition oscilloscope. We configure it to capture a signal with 10 Giga sample per second and record the samples in a file for further analysis. As the frequency range of this oscilloscope is 0–2.5 GHz, we use a frequency down converter to move the received IEEE 802.11ad frames to baseband, using a SiversIMA FC2221V/01 V-band converter. To capture the reflections from an object, we have to use a full-duplex system. As there is no 802.11ad device that is full duplex, therefore we have to use a separate receiver beside the transmitter in our experiments. A Dell D5000 mmWave docking station (number 3 in Figure 3) is used as a mmWave transmitter. It is a WiGig device, which for our purposes is the same as 802.11ad since it uses the same Golay sequences. When it is turned on, it tries to find a Dell laptop with IEEE 802.11ad functionality to connect to by sending 32 beacons in 32 different directions. These are modulated using a basic but robust binary phase shift keying (BPSK) modulation. The signal propagates directly and is reflected by the reflector (number 1 in Figure 3) and received by the SiversIMA down converter equipped with a horn antenna (number 2 in Figure 3) which is controlled by a dedicated software (number 5 in Figure 3). The down-converted signal is fed to the oscilloscope which is used to capture the signal. We trigger the oscilloscope to capture the received signal from the down-converter. As the transmitter periodically transmits 32 beacon frames, the oscilloscope can show an almost constant signal shape. The captured signal is decoded and analyzed by the Agilent 81199A Wideband Waveform Center software (number 6 in Figure 3). This software produces several outputs for each frame it detects in the decoded signal including the data frame content, the constellation map, and the channel estimation.

By writing a computer code, we automate the decoding process of the 81199A software for multiple captured signals, to decode all included frames. It uses the transmission control protocol (TCP) server connection provided by the 81199A software to communicate with the software. The rest of this section explains our experimental setups and results.

4.1 Experiment 1: Reflections From Different Objects

In this experiment, we first use the setup shown in Figure 3. We use two different horn antennas, with 20° and 7° beam widths. We also use two objects as reflector: a metal PC case (shown in Figure 3), and an empty paper box. Then we change the distance of the reflector from the transmitter-receiver set, capture the reflected signal, record it with the Oscilloscope, and analyze it by the 81199A software.

We then set up further experiments in other indoor environments to measure the reflections from other objects from different distances. We use glass wall, brick wall, wooden wall (in an indoor environment) and a metal door (in a corridor) as reflectors and repeat the same experiments using the 7° beam width horn antenna. In our experiment in the corridor, the maximum distance from the end of corridor at which we can trigger the oscilloscope is 24 meters. The up/down convertor adds some noise to the signal which makes the signal quality worse with respect to a commercial receiver. So, we expect to receive the reflections from longer distances in commercial devices.

Figure 4 shows the normalized CIR of beacon frames measured by the 81199A software, when we use a brick wall as the reflector. The largest peak in each signal corresponds to the direct reception by the receiver which corresponds to distance zero. The second largest peak corresponds to the reflection from the wall (see Figure 2). The distance between these two peaks corresponds to the twice the distance between the transmitter/receiver and the reflector. The blue star in each figure shows the expected location of the peak

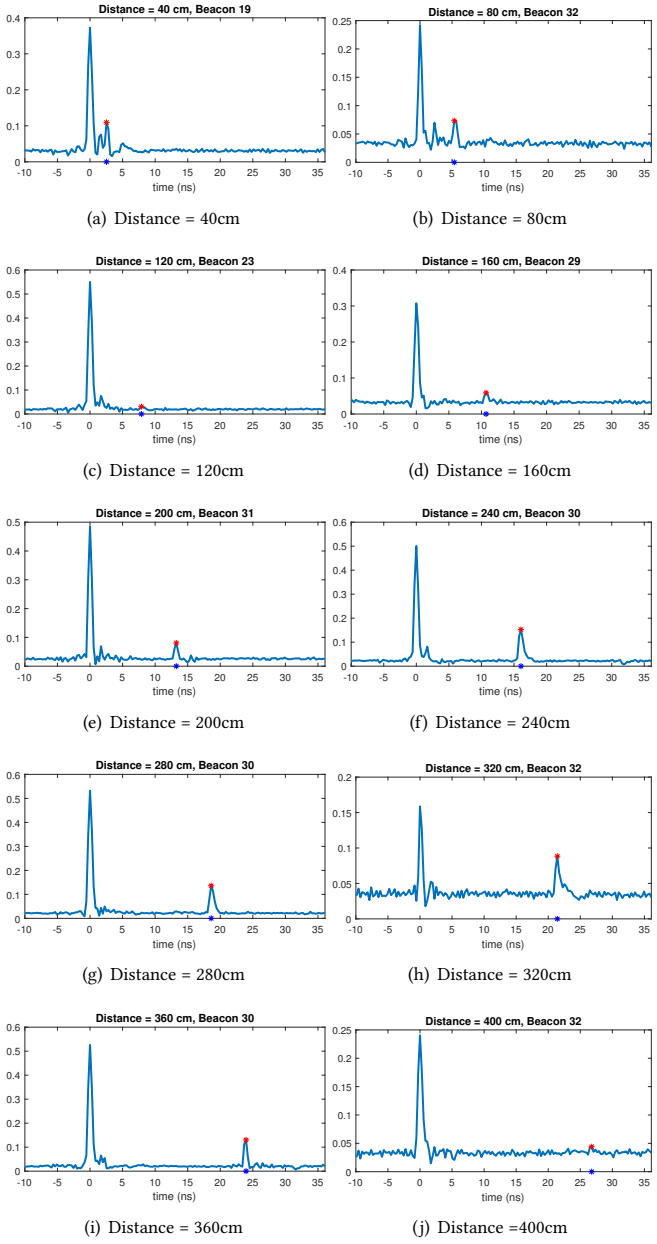

(a) Distance = 40cm (b) Distance = 80cm

(c) Distance = 120cm (d) Distance = 160cm

(e) Distance = 200cm (f) Distance = 240cm

(g) Distance = 280cm (h) Distance = 320cm

(i) Distance = 360cm (j) Distance =400cm

Figure 4: CIR of beacon frames: Reflection by a brick wall from different distances in the lab environment using 7° horn antenna. Blue stars: expected location for peak, red stars: detected peak.

based on the light speed formula: $\Delta t = \frac{2d}{c}$, where Δt is the time difference between the two peaks, d is the distance between the transmitter/receiver and the reflector, and c is the speed of light. As in each experiment, d is known, we can compute Δt, which is the location of blue stars. It is notable that, we know d for our evaluation, but a real system using this technique would actually

Table 1: Absolute Error in Experiment 1

Exp.	Absolute Error (E) in cm at Different Distances (D)									
Brick	D (cm)	40	80	120	160	200	240	280	320	360	400
	E (cm)	1.9	0.3	1.6	0.7	1.3	1.0	0.9	1.3	0.6	1.7
Glass	D (cm)	50	100	150	200	250	300	350	450	500	
	E (cm)	0.7	1.5	2.0	1.3	0.5	4.4	45.6	6.6	3.1	
Wood	D (cm)	50	75	100	125	150	175	200	225		
	E (cm)	0.7	1.1	1.5	1.8	2.0	1.6	1.3	0.9		

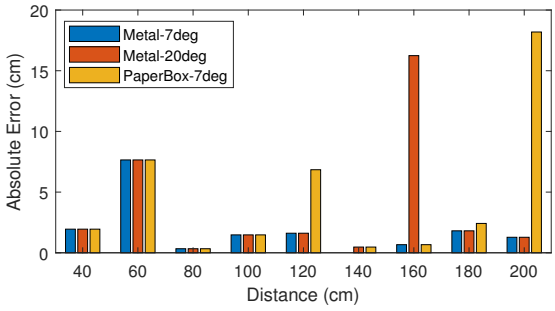

Figure 5: The absolute error for the measured distance: Reflection by a metal and paper box from different distances in the lab environment using 20° and 7° horn antennas.

determine d based on the measurement. The red star in each figure shows the detected maximum in the signal after the first peak.

Note that, in each experiment we record a signal containing 32 beacon frames, from which a subset of them could be decoded by the 81199A software. From all decoded frames, we choose one with the minimum distance error which its number is written in the title of each plot. Indeed, in practice we can choose the best beacon based on their beam-patterns. However, as we expect to have more directional antenna patterns in near future with respect to current antenna patterns, we use the best beacon here as a proof of concept for the idea, hoping that in future the chosen antenna pattern has the required beam-pattern designed for this purpose. The first row of Table 1 shows the absolute error of our method corresponding to red stars in Figure 4 in cm. In this table, D and E stand for distance and absolute error, respectively. So for example, the measured error at distance 400 cm is 1.7 cm. As can be seen, the maximum error here is less than 2 cm.

Figure 5 shows the absolute error for the measured distance in the setup of Figure 3, comparing measurement error when using the metal and paper box as reflector from different distances in the lab environment using 20° and 7° horn antennas. Here the maximum error is less than 20 cm. Comparing blue and red bars, we observe that use of more directional antenna (7° beamwidth) makes more precise results with respect to wider beamwidth antennas, in particular, at distance 160 cm the error of using a wide beamwidth antenna (20° beamwidth) is about 17 cm, while the error for the more directional antenna (7° beamwidth) is less than 2 cm. This reveals the importance of directionality of the array antenna beamwidth. Also, comparing blue and yellow bars, we

(a) The environment and the experimental setup.

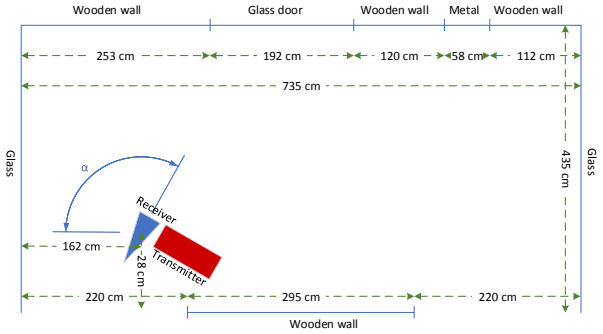

(b) The environment map. $\alpha \in \{0^\circ \cdots 180^\circ\}$.

Figure 6: Experimental setup to test the feasibility of 2D modeling of an environment.

observe the distance error with paper box is larger than that of metal as expected, as the metal is a better reflector.

By conducting similar experiments using wooden and glass walls as reflectors, we summarize the distance measurement error in the 2nd and 3rd rows of Table 1. For example, the measurement error at distance 50 cm is 0.7 cm in both experiments. Here the maximum error is 45 cm when using glass as reflector at distance 350 cm. These are outliers in our measurements. The source of such errors are reflections from other objects in the vicinity which create a larger peak compared to the main reflector in our experiment. It is possible to find the source for these peaks and separate them by more advanced signal processing. However, in this paper we aim at showing the feasibility of measuring the distance from an object and to make a 2D model of the environment based on this measurement.

4.2 Experiment 2: 2D Modeling of a Room

To check the feasibility of 2D modeling of the environment, we set up an experiment in an indoor environment using the horn antenna with 7° beam width. The environment and our experimental setup is shown in Figure 6–a. In Figure 6–b, we sketch the map of our experiment. We put the transmitter and receiver beside each other and change the angle of transmission/reception from 0° to 180°. The

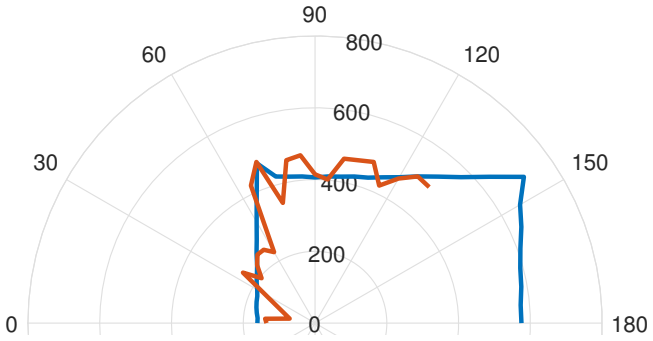

Figure 7: The 2D model measured based on the computed distances in each angle. Blue line: the ideal ranging, red line: measured ranging. (Units of radius are in cm.)

transmitter transmits 32 beacons in different directions. The signal is reflected from the walls and received by the receiver. By changing the angle of transmission/reception toward different directions, we measure the distance from the wall and develop a 2D model similar to the map in Figure 6–b in the next section.

Figure 7 shows the 2D model we make based on the measurements we do in this experiment at different angles. The blue and red line correspond to the blue and red stars in Figure 4, respectively. The 81199A software measures the channel estimation based on some sort of decision feedback equalization (DFE) of the channel and it sets the maximum delay to 36 ns based on the length of the equalizer, and therefore, in this software, this value cannot be changed. This means that the maximum measurable distance of an object is 5.4 m ($36 \times 10^{-9} \times 3 \times 10^8/2$), a limitation by the 81199A software in our experiments, and not by the IEEE 802.11ad standard. This is why we can not extend the model to degrees beyond 120°. This figure proves the feasibility of our hypotheses on 2D modeling of the environment based on the reflections of mmWave. This can also be extended to a 3D model by using more directional antennas directed toward 3D directions. It is notable that this 2D model can be made better with less error by doing more measurements, and in particular, from different locations in the room. Also, note that the error is smaller when the direction of transmission is perpendicular to the surface of the object, i.e., at 0°, 90°, and 180°. None of the frames between angles $15^\circ \cdots 30^\circ$ is decoded, because of low signal energy with respect to the noise level. This is due to the Newton's law of light reflection. Referring to Figure 6–b, these angles correspond to non-perpendicular reflection from glass which is a good reflector. It means that, we cannot receive enough energy with this method when we try to detect good reflectors while their surface is not perpendicular to the transmission line of the electromagnetic wave. However, this can be solved by taking measurements from multiple locations, which is possible in practice with multiple access points (AP), or by receiving measurements from UE moving in the environment.

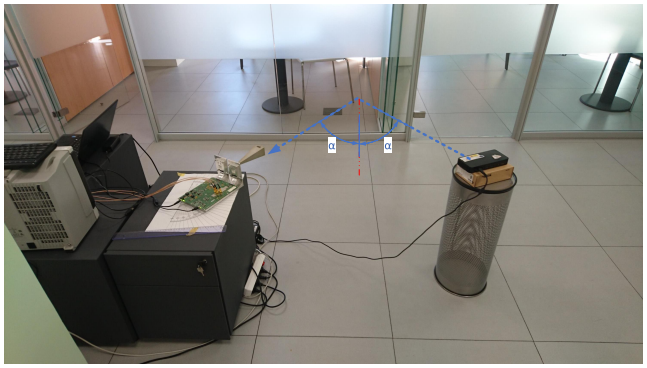

Figure 8: The experiment setup to observe the Newton's law of light reflection for mmWave propagation reflected from glass. The transmitter and receiver are located in two different points directed toward the glass wall with the same angle α from the perpendicular line.

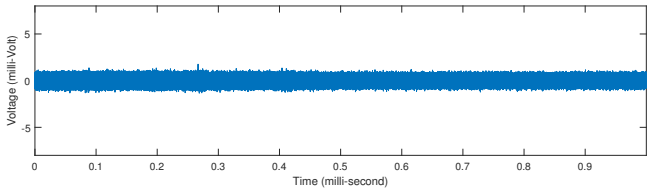

(a) Experiment 2, Setup of Figure 6, Angle = 20°

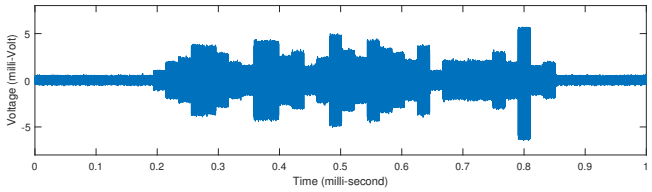

(b) Experiment 3, Setup of Figure 8, Angle = 20°

Figure 9: Time domain signal of beacon frames in Experiment 3 compared with Experiment 2. Received signal quality when the receiver is located (a) exactly beside transmitter; (b) in a location which receives the reflected signal from the glass according to Newton's law of light reflection.

4.3 Experiment 3: Newton's Law of Light Reflection

In the experiment setup of Section 4.2 we observe that the reflected signal from the glass cannot be captured in some angles. This means that when the mmWave is propagated to a good reflector, it follows the Newton's law of light reflection. So, when the transmitter and receiver are in the same location, and the transmitter propagates with an angle not perpendicular to the reflector, the reflected signal cannot be received by the receiver. We set up another experiment to prove this. Figure 8 shows this setup. Here, the transmitter and receiver are located in two different points separated from each other and both are directed toward the glass wall as a good reflector with the same angle from the perpendicular line. The reflected signal is received by the receiver and decoded correctly, while it can not be received when we put the receiver beside the transmitter.

Figure 9 shows the signal in the time domain for different beacon frames in Experiment 3 (Figure 9–b) compared with Experiment 2 (Figure 9–a). Both figures show the captured signals in the time domain which depict 32 beacon frames transmitted in 32 different directions. Comparing these plots, we observe that the signal in this experiment is more powerful. This suggests that the mmWave electromagnetic wave follows the Newton's law of light reflection, when it is reflected by a smooth surface good reflector. This can make some issues when trying to make 2D/3D models of the environment as reported in Section 4.2.

4.4 Experiment 4: Direct Communication From Different Angles

In this experiment, we put the transmitter and receiver 2 meters away and align their antenna facing each other. We change the angle of transmitter from $-90^\circ \cdots + 90^\circ$, where 0° means both antennas are facing exactly toward each other. We use the big horn antenna with 7° beam width for the receiver. This way, we can measure the received signal power and measure antenna patterns for different directions. The measurements are done in the same environment of Figure 3. So, the measured patterns are related to this environment.

Referring to Figure 9–b we observe that the power level of all 32 beacons are significant, which means that the side-lobes of each antenna pattern of the Dell docking station are big enough so that the receiver can receive from all antenna patterns. This means that the antenna patterns are not directional enough, proving they have non-directional patterns. In the other words, by aligning the receiver horn antenna to all directions, we can still receive and decode almost all beacon frames which are supposed to be transmitted toward a single direction. If the transmitter antenna was ideal, we can only receive from a few directions and the shape of signal in Figure 9–b is expected to contain a few peaks (signals with enough energy), rather than 32 peaks.

For measuring signal-to-noise ratio (SNR), by using a computer code, we automatically find the margins of beacon frame signals using the signal power level applying a sliding window method. After finding the beacon frame signal margins, we measure the signal plus noise power. We also measure the noise power from the first part of signal knowing only noise exists there. By subtracting noise power from the measured power in a region containing beacon frame (which contains the signal plus noise), we obtain signal power. By dividing signal power to the noise power measured this way, we obtain SNR, which we call it measured SNR in this paper.

In Figure 10, we show some sample antenna patterns based on the measured SNR (blue lines) and based on the SNR read from the 81199A software (red line) in dB (logarithmic values). We normalize both SNR values to make them have similar scales for the sake of better visibility. Therefore, the values on the r axis show relative SNRs which include a constant bias added to all SNRs. As can be seen, both methods show almost similar antenna patterns. Since it is not known how the 81199A software measures the SNR, it is not possible to find the reason for the difference between these two

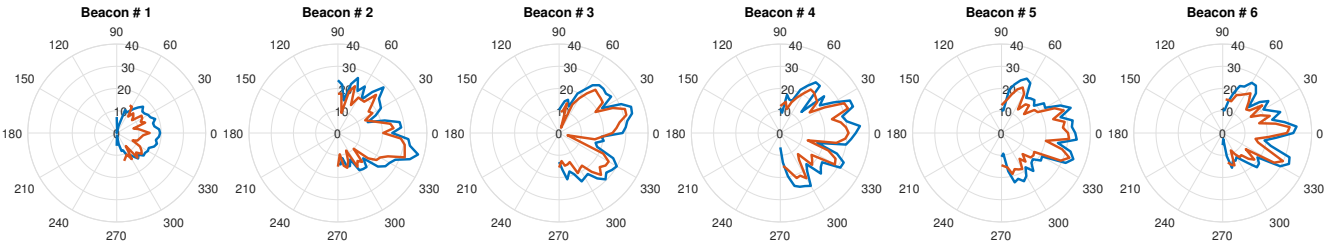

Figure 10: Sample antenna patterns of beacon frames based on our measured normalized SNR (blue) and the normalized SNR read from the 81199A software (red).

measurements. However, at this stage, it is not important to know the cause of the difference, and the overall patterns which are not directional are important for us. In the other words, none of the patterns are directional in a single direction. Most of them have multiple main lobes.

Note that some patterns such as that for beacon 1 are very small patterns, without any directionality. These patterns may have their lobes in other planes in a 3D pattern. Steinmetzer et al. [18] measured the antenna pattern of Talon routers in an anechoic chamber and showed similar results, but with more detailed patterns.

5 OBSERVATIONS AND CHALLENGES

In this section, we summarize our main observations from the experiments we explained in the previous sections. We also discuss the main challenges that we believe we need to address when we want to make a 2D/3D model of the environment by using mmWave radar detection potential.

5.1 Observations

Our main observations are as follows:

(1) It is feasible to measure the distance of an object from a mmWave transmitter device by using the measured CIR of the IEEE 802.11ad frames.
(2) Some objects show better reflection properties, such as metal and glass, but even a poor reflector such as an empty paper box reflects enough energy to be detected.
(3) The objects with non-smooth surfaces such as human body scatter the wave and our setup fails to detect them. Using down-converters adds a considerable amount of noise and makes the detection impossible. However, within a commercial device, this problem can be solved, as it is possible to receive enough energy with less noise.
(4) It is feasible to make a 2D/3D model of the environment using the radar detection potential of mmWave.
(5) The commercial mmWave transmitters have non-directional antenna patterns with multiple main lobes.
(6) When the mmWave electromagnetic wave is reflected from a good reflector with a surface not perpendicular to the direction of wave propagation, the reflection of mmWave follows Newton's law of light reflection. So, its reflection cannot be received by the receiver.
(7) This approach is highly dependent on the decoding of the reflected wave. It fails when the noise level is high or when the CIR cannot be estimated correctly. This limits its applications. However, we expect that with frequency modulated continuous wave (FMCW) method [19] we can detect the objects for difficult environmental conditions.

5.2 Challenges

We summarize the main challenges that should be addressed when we want to make a 2D/3D model of the environment by using mmWave ranging potential as follows:

(1) Using the preamble of IEEE 802.11ad frames is an economic way for detecting objects as it uses the same electronic circuitry. However, the radio frequency (RF) module should work in full-duplex, i.e., it should receive simultaneously with its transmission. We can use the FMCW chipset instead, which is designed for this purpose, or check if this can be included in the IEEE 802.11ad chipsets.
(2) The commercial mmWave transceivers have antenna arrays with non-directional antenna patterns including multiple main lobes. This makes the ranging problem hard or even impossible, because we cannot distinguish from which direction we receive a signal. On the other hand, these antenna patterns have small antenna gains which prevents the devices from being able to operate with higher modulation/coding schemes and so, with higher bit-rates. Hence, this is an important problem for data communication as well, and they are also trying to address it. In theory, they need more antenna elements to make more directional patterns. However, even with non-ideal antennas, we believe that it is still possible to detect objects, but with processing lots of information. Considering that the antenna patterns are 3D, this makes the problem even harder.
(3) mmWave propagation follows the Newton's law of light reflection when it is reflected by a smooth surface reflector. This prevents any reception from these reflectors when the angle of incidence is not perpendicular to the surface of the reflector. This limits the view of fixed devices such as access points and base stations. However, considering that the UEs with mmWave potential can share their information from the reflections they receive from different objects with the AP, this problem can be addressed.
(4) To detect small objects and objects with an uneven surface such as human body, the transceiver should be close to the

object. This also can be addressed by using the recorded data from the UEs.

(5) Fitting the images made by the reflections received by the UEs to the image made by the AP is also a challenging problem.

(6) Processing the big-data generated from the reflections reported by millions of UEs and using them to update the 2D/3D model or make it more precise is another main challenging problem. In particular, when we try to combine the information from different types of devices with different antenna patterns, with different precisions, and with different methods (such as processing of IEEE 802.11ad and FMCW).

6 CONCLUSION AND FUTURE WORK

In this paper, we report the details of our experiments with a mmWave testbed, and show the feasibility of IEEE 802.11ad for mmWave ranging with communication equipment. We provide our main observations and summarize the main challenges that should be addressed when we try to make a 2D/3D model of the physical environment. Our results show a precision of 2 cm in most experiments. We also make a 2D model of an indoor environment by this method, which shows the feasibility of our hypotheses.

The proof of feasibility of using mmWave detection for mmWave communication is an important achievement which can be used to enhance communication performance in mmWave frequency range and to provide new tools for enhancing antenna tracking and training protocols. It also can lead us to make a 2D/3D model of the environment which is an important achievement useful for smart cities/buildings applications. So, our plan for future work is to extend our experiments in particular with FMCW method and to focus on addressing the challenges mentioned in this paper.

REFERENCES

[1] Omid Abari. 2017. Enabling High-Quality Untethered Virtual Reality. In *Proceedings of the 1st ACM Workshop on Millimeter-Wave Networks and Sensing Systems 2017 (mmNets '17)*. ACM, New York, NY, USA, 49–49.

[2] H. Ajorloo and M.T. Manzuri-Shalmani. 2013. Modeling Beacon Period Length of the UWB and 60-GHz mmWave WPANs Based on ECMA-368 and ECMA-387 Standards. *Mobile Computing, IEEE Transactions on* 12, 6 (June 2013), 1201–1213.

[3] H. Ajorloo and M. T. Manzuri-Shalmani. 2016. Throughput Modeling of Distributed Reservation Protocol. *IEEE Transactions on Mobile Computing* 15, 2 (Feb 2016), 503–515.

[4] M. Bocquet, C. Loyez, M. Fryziel, and N. Rolland. 2012. Millimeter-wave broadband positioning system for indoor applications. In *2012 IEEE/MTT-S International Microwave Symposium Digest*. 1–3.

[5] X. Cui, T. A. Gulliver, J. Li, and H. Zhang. 2016. Vehicle Positioning Using 5G Millimeter-Wave Systems. *IEEE Access* 4 (2016), 6964–6973.

[6] Ryan Dobbins, Saul Garcia, and Brian Shaw. 2011. *Software Defined Radio Localization Using 802.11-style Communications*. Bachelor thesis. Worcester Polytechnic Institute, USA.

[7] X. Guo and N. Ansari. 2017. Localization by Fusing a Group of Fingerprints via Multiple Antennas in Indoor Environment. *IEEE Transactions on Vehicular Technology* 66, 11 (Nov 2017), 9904–9915.

[8] Texas Instruments. 2018. Short-range radar mmWave sensors. http://www.ti.com/sensors/mmwave/overview.html

[9] L. Kong, M. K. Khan, F. Wu, G. Chen, and P. Zeng. 2017. Millimeter-Wave Wireless Communications for IoT-Cloud Supported Autonomous Vehicles: Overview, Design, and Challenges. *IEEE Communications Magazine* 55, 1 (January 2017), 62–68.

[10] P. Kumari, J. Choi, N. GonzÃąlez-Prelcic, and R. W. Heath. 2018. IEEE 802.11ad-Based Radar: An Approach to Joint Vehicular Communication-Radar System. *IEEE Transactions on Vehicular Technology* 67, 4 (April 2018), 3012–3027.

[11] F. Lemic, J. Martin, C. Yarp, D. Chan, V. Handziski, R. Brodersen, G. Fettweis, A. Wolisz, and J. Wawrzynek. 2016. Localization as a feature of mmWave communication. In *2016 International Wireless Communications and Mobile Computing Conference (IWCMC)*. 1033–1038.

[12] Z. Lin, T. Lv, and P. T. Mathiopoulos. 2018. 3-D Indoor Positioning for Millimeter-Wave Massive MIMO Systems. *IEEE Transactions on Communications* 66, 6 (June 2018), 2472–2486.

[13] W. Liu, F. Yeh, T. Wei, C. Chan, and S. Jou. 2013. A Digital Golay-MPIC Time Domain Equalizer for SC/OFDM Dual-Modes at 60 GHz Band. *IEEE Transactions on Circuits and Systems I: Regular Papers* 60, 10 (Oct 2013), 2730–2739.

[14] V. Nambiar, E. Vattapparamban, A. I. Yurekli, I. Guvenc, M. Mozaffari, and W. Saad. 2017. SDR based indoor localization using ambient WiFi and GSM signals. In *2017 International Conference on Computing, Networking and Communications (ICNC)*. 952–957.

[15] A. Olivier, G. Bielsa, I. Tejado, M. Zorzi, J. Widmer, and P. Casari. 2016. Lightweight Indoor Localization for 60-GHz Millimeter Wave Systems. In *2016 13th Annual IEEE International Conference on Sensing, Communication, and Networking (SECON)*. 1–9.

[16] T. S. Rappaport, S. Sun, R. Mayzus, H. Zhao, Y. Azar, K. Wang, G. N. Wong, J. K. Schulz, M. Samimi, and F. Gutierrez. 2013. Millimeter Wave Mobile Communications for 5G Cellular: It Will Work! *IEEE Access* 1 (2013), 335–349.

[17] A. Shahmansoori, G. E. Garcia, G. Destino, G. Seco-Granados, and H. Wymeersch. 2018. Position and Orientation Estimation Through Millimeter-Wave MIMO in 5G Systems. *IEEE Transactions on Wireless Communications* 17, 3 (March 2018), 1822–1835.

[18] Daniel Steinmetzer, Daniel Wegemer, Matthias Schulz, Joerg Widmer, and Matthias Hollick. 2017. Compressive Millimeter-Wave Sector Selection in Off-the-Shelf IEEE 802.1 Lad Devices. In *Proceedings of the 13th International Conference on Emerging Networking EXperiments and Technologies (CoNEXT '17)*. ACM, 414–425.

[19] A. G. Stove. 1992. Linear FMCW radar techniques. *IEE Proceedings F - Radar and Signal Processing* 139, 5 (Oct 1992), 343–350.

[20] J. Talvitie, M. Valkama, G. Destino, and H. Wymeersch. 2017. Novel Algorithms for High-Accuracy Joint Position and Orientation Estimation in 5G mmWave Systems. In *2017 IEEE Globecom Workshops (GC Wkshps)*. 1–7.

[21] Agilent Technologies. 2013. Agilent Wideband Waveform Center 81199A. User's Guide. https://literature.cdn.keysight.com/litweb/pdf/81199-91020.pdf

[22] Agilent Technologies. 2013. Wireless LAN at 60 GHz - IEEE 802.11ad Explained: Application Note. White Paper.

[23] Zhicheng Yang, Parth H. Pathak, Yunze Zeng, Xixi Liran, and Prasant Mohapatra. 2016. Monitoring Vital Signs Using Millimeter Wave. In *Proceedings of the 17th ACM International Symposium on Mobile Ad Hoc Networking and Computing (MobiHoc '16)*. ACM, New York, NY, USA, 211–220.